Examination of a High Redshift Quasar and its Host Galaxy

A Senior Honors Thesis

Presented in Partial Fulfillment of the Requirements for graduation *with research distinction* in Astronomy in the undergraduate colleges of The Ohio State University

by

Nathaniel R. Ross

The Ohio State University
June 2009

Project Adviser: Professor Christopher S. Kochanek, Department of Astronomy

ABSTRACT

We have measured the spectral energy distribution (SED) of the host galaxy of the $z_s = 1.7$ gravitationally lensed quasar SDSS J1004+4112 from $0.44-8.0\mu$m ($0.16 - 3.0\mu$m in the rest frame). The large angular extent of the lensed images and their separation from the central galaxy of this cluster lens allows the images to be resolved even with the Spitzer Space Telescope. Based on the SED, the host galaxy is a mixture of relatively old and intermediate age stars with an inferred stellar mass of $\log(M_\star/M_\odot) = 11.09 \pm 0.28$ and a star formation rate of $\log(\dot{M}/\mathrm{M}_\odot\ \mathrm{yr}^{-1}) = 1.18 \pm 0.26$. Given the estimated black hole mass of $M_{BH} \simeq 10^{8.6}\mathrm{M}_\odot$ from locally-calibrated correlations of black hole masses with line widths and luminosities, the black hole represents a fraction $\log(M_{BH}/M_\star) = -2.49 \pm 0.28$ of the stellar mass and it is radiating at 0.24 ± 0.05 of the Eddington limit. The ratio of the host stellar mass to the black hole mass is only marginally consistent with the locally observed ratio.

1. Introduction

In the local universe, the host galaxies of active, luminous black holes tend to be bluer star forming galaxies with a roughly 1000:1 ratio between star formation and accretion rates (Kauffmann & Heckman 2005). More luminous AGN also show younger stellar populations. Moreover, the relative growth rates match the observed local ratio of stellar to black hole mass (Kauffmann & Heckman 2005; Marconi & Hunt 2003). At higher redshifts, $z > 1$, the picture is less clear because the greater distances and higher typical AGN luminosities make it increasingly difficult to study host galaxies. Studies by Peng et al. (2006a,b) argue that the relationship is shifted and that at this epoch ($z > 1$) the black hole mass grows faster relative to the stellar mass than is observed locally, while Lauer et al. (2007) and Di Matteo et al. (2008) argue for little change.

There is also considerable interest in the star formation rates of the hosts at these redshifts. With the now prevalent view that the black holes and stars grow in a self-regulating process (e.g. Hopkins et al. 2005a,b, 2006; Sijacki et al. 2007; Di Matteo et al. 2008), particularly during major mergers, it is of considerable importance to be able to estimate both the stellar mass and the star formation rate. In the Hopkins et al. (2005a,b) scenario, the peak star formation rates precede the peak quasar luminosity, and the quasar phase lasts about 10^7 years. Unfortunately, estimating both stellar masses and star formation rates at these redshifts requires not only a detection of the host but a reasonably complete spectral

energy distribution (SED).

Here we make use of gravitational lensing to measure the SED of a $z_s = 1.73$ quasar host galaxy from 0.44–8.0μm and infer its mass and star formation rate. As emphasized by Peng et al. (2006b), quasar lenses are ideal laboratories for studies of quasar hosts because the lens magnification "pulls" the host out from under the quasar to provide a $\sim 10^2$ improvement in contrast. Moreover, the arced shapes of the lensed hosts are easily distinguished from PSF artifacts. Our target is the five image lens SDSS J1004+4112 (Inada et al. 2003, 2005; Sharon et al. 2005; Ota et al. 2006; Fohlmeister et al. 2007, 2008; Inada et al. 2008). This lens is created by a $z_l = 0.68$ cluster of galaxies (Inada et al. 2003), giving it exceptionally large image separations (a ~ 14 arcsec Einstein ring diameter) that both lead to very large images of the host and places the quasar images well away from the lens galaxy emission. In fact, the host is so extended and well-separated from the lens that it can be resolved by the Spitzer Space Telescope with relative ease. There are also additional, higher redshift lensed galaxies (Sharon et al. 2005) and time delay measurements of $\Delta\tau_{BA} = 40.6 \pm 1.8$ days, $\Delta\tau_{CA} = 821.6 \pm 2.1$ days, and $\Delta\tau_{AD} > 1250$ days between A/B, A/C, and A/D images, respectively (Fohlmeister et al. 2008). In §2 we describe how we measure the spectral energy distribution (SED) of the host galaxy and the quasar. In §3 we use these estimates to determine the luminosity, stellar mass, and star formation rate of the host galaxy. We assume a flat, $\Omega_0 = 0.3$, $H_0 = 70$ km/s/Mpc cosmology.

2. Data

We use Hubble Space Telescope (HST) and Spitzer Space Telescope (SST) observations of SDSS J1004+4112 in 8 bands covering the visual to mid-infrared wavelengths. The HST data consists of ACS/WFC B(F435W), V(F555W), I(F814W) observations and NICMOS/NIC2 H(F160W) observations. The SST/IRAC data consists of 3.6, 4.5, 5.8, and 8.0μm observations. For the V, I, H, and IRAC bands we have multiple observational epochs. A summary of the observations is given in Table 1. Each observation consists of several sub-exposures, drizzled together (Fruchter et al. 2002) to create one background-subtracted image. We later use background apertures to correct for any mis-estimation of the background, and include it in our error estimates.

We first used a parametric model to fit the images using a combination of point sources for the quasars, exponential disks and de Vaucouleurs models for the cluster galaxies and Gaussians for the images of the host galaxies, all convolved with point spread function (PSF) models, as in Lehár et al. (2000). These have problems for estimating the flux of the host galaxy due to the fact that the PSF, generated by TinyTim for the HST bands and obtained

from SST for the IRAC bands, has significant fractional errors at the peak of the quasar, exactly where the model for the host galaxy also peaks. The parametric models tend to overestimate the flux of the host galaxy in order to reduce the residuals at the position of the quasar. We will use these models only to correct aperture magnitudes for the effects of the point spread function.

We next created a series of masks which isolate regions on the images where the flux is dominated by either the host galaxy or the quasar, in both cases excluding flux from objects in the field. These masks have regions with value either 0 or 1 in order to exclude or include flux in specific pixels when multiplied into the original images. We keep the masks consistent across all bands by geometrically transforming a master copy to the appropriate centering, pixel scale, and orientation of each observation. We defined three types of masks. Host masks exclude flux both near the quasars and away from the host images seen in the I/H data. Quasar masks include only flux near the peak of the quasar images. Background masks include a region outside the host mask which we use to estimate any residual background flux. Joint masks combine the host and the quasar masks to estimate the total flux of both components. Figure 1 superposes these masks on an H-band image.

When we apply a mask to a region, we calculate the flux f_{mask} under the mask. This flux is a combination of the true flux in the masked region f with contamination f_{cont} spread into the masked region by the PSF, losses f_{loss} out of the region due to the PSF, and f_{back} due to any mis-estimation of the background during the image reduction process. For example, we estimate f_{cont} and f_{loss} for our host mask as follows. We start from the model of the image without PSF convolution. We then mask this image, convolve it with the PSF, and measure the flux under the second mask. Thus the contamination, f_{cont}, of the host mask region due to the PSF spreading flux out of the quasar mask region, is found by first masking the unconvolved model image with the quasar mask, convolving this masked image with the PSF, and then measuring the flux found in the host mask region, while f_{loss} is found by masking with the host mask, convolving with the PSF and then measuring the flux outside of the host mask. Since these corrections are modest, we are not very sensitive to the problems in the model image. We estimate the background by subtracting the model from the data and measuring the residuals in the background mask. The resulting flux for any region is then

$$f \;=\; f_{mask} \;-\; f_{cont} \;+\; f_{loss} \;-\; f_{back} \tag{1}$$

The measurements are summarized in Table 2. We first estimate statistical uncertainties in the magnitudes using a bootstrap resampling of the images. The bootstrap resampling technique creates an ensemble of trial images by sampling with replacement from the sub-images (dithers, CR Splits, etc.) that were averaged together for each observation. We analyze each trial image in the same manner as the true images and estimate error bars

from the variance of the results over the trials. The remaining uncertainty arises from the background subtraction. We recompute all the estimates using two different regions for estimating the background flux, as well as a background estimate generated by the model fits. The dispersion of these background estimates, multiplied by the number of pixels in a given mask region, gives an estimate of the background uncertainties in each mask region. Small changes in the estimated background can have significant effects on the flux measured for the host because of the large number of pixels in both the host mask and the joint mask. The uncertainties we present in Table 2 are a combination of these statistical and background uncertainties, added in quadrature.

We use data from the ongoing monitoring of SDSS J1004+4112 (Fohlmeister et al. 2008) to correct for time variability of the quasar in the QSO and joint masks. We chose 13 December 2005 as the reference date, as many of our observations were made close to this date (see Table 1). We estimate the time delay corrections by comparing the flux measured in the monitoring project on or within 2 days of the observation with the flux measured in the monitoring project on or within 2 days of the reference date. These time delay corrections range from about 0.05 to −0.44 magnitudes. We use these time delay corrections only for the optical to near-IR observations of the quasar because the observations in the mid-IR show much less variability, as one would expect from the general trend of reduced variability at longer wavelengths (e.g. Vanden Berk et al. 2004). We do not correct for the time delays between the lensed images because the image D time delay is not known (see Fohlmeister et al. 2008). Essentially, we will "time average" the properties of the quasar in our final results.

3. Analysis

We used an extended version of the SED template models presented by Assef et al. (2008) to fit the data for each lensed image. These templates consist of early-type, Sbc, Irr and QSO templates empirically derived by fitting the GALEX UV through SST/MIPS 24μm SEDs of 13623 "pure" galaxies (with no obvious signatures of nuclear activity) and 4242 quasars and galaxies with AGN activity in the NDWFS Boötes field (Jannuzi & Dey 1999), with redshifts measured by the AGN and Galaxy Evolution Survey (AGES, Kochanek et al. in prep.). Assef et al. (2008) details the procedure used to derive these templates, and they will be discussed in depth in an upcoming paper by Assef et al. (2009).

For images A, B, and C we separately fit the host, QSO and joint SEDs, while for image D we only fit the joint SED. Figures 2, 3, and 4 show examples of the template fits and Table 3 lists the host luminosities derived from the template fits to the host, QSO, and joint mask

data. These luminosities are corrected for magnification by the lens using magnifications of 28.5, 19.1, 9.8, 7.8 for the A, B, C, and D images, respectively, from the models of Inada et al. (2008; Oguri, private communication).

We used several methods to estimate our systematic uncertainties in determining the properties of the host galaxy. First, we fit the host mask data both with and without the B-, V-, and I-band data in order to examine the effect of eliminating the data points with the worst signal-to-noise ratios. These fits produced significant variations on an image by image basis, but showed little effect on the averages. Next we fit the QSO and joint mask data once by allowing all template components to vary and once by fixing the ratios of the galaxy templates using the results of the host mask fits. These fits produced different results for the template ratios (although the Irr template was never favored) and the joint fits have systematically brighter host and fainter AGN components than the simple sum of the separate host and quasar mask results, but these variations had no significant effect on the luminosities, masses, or star formation rates.

We use the template fits and standard scaling relations to estimate the stellar mass and star formation rate of the host galaxy. We use the estimated rest frame 8.0μm flux of the host to estimate the total infrared luminosity based on the scalings of Bavouzet et al. (2008), which in turn is used to estimate the star formation rate (SFR)

$$\frac{SFR}{1\mathrm{M}_\odot\,\mathrm{yr}^{-1}} = \frac{L_{FIR}}{5.8\times10^9\mathrm{L}_\odot} \tag{2}$$

of the host galaxy using the local scalings of Kennicutt (1998), corrected for the difference in the definition of the total infrared luminosity between Bavouzet et al. (2008) and Kennicutt (1998). The uncertainties in the star formation rates are dominated by the uncertainties in extrapolating to the total infrared luminosity from the 8.0μm flux. Bavouzet et al. (2008) found a 38% scatter between the 8.0μm flux and L_{FIR}, while Kennicutt (1998) found a scatter of about 30-50% between the L_{FIR} and the SFR, and also attributed it to the uncertainty in estimating the FIR luminosity from the near infrared luminosity and uncertainty in the effects of extinction.

We combined the template models with the results of Bell et al. (2003) to estimate the stellar mass of the host galaxy. Bell et al. (2003) assumed a universal "diet Salpeter" Initial Mass Function (IMF) and a variety of star formation histories to simulate SED templates, which they then fit to a large sample of SDSS galaxies to estimate mass-to-light ratios as a function of rest frame colors. They took these M/L ratios, in combination with the measured colors of the galaxies, to derive relationships between colors and mass-to-light ratios, $\log(M/L) = a_\lambda + (b_\lambda\times\mathrm{color})$, as detailed in Bell et al. (2003) (Table 7). We assume a Kroupa IMF, which better represents a normal stellar population, and this introduces a

-0.15 dex correction to the value of a_λ. We estimate the rest frame $(g-r)$ color and K-band luminosity from our template fits, and then use the Bell et al. (2003) K-band parameters ($a_K = -0.359$ and $b_K = 0.197$) to estimate the mass-to-light ratio. This leads to an estimated host K-band $\log(M/L) = (-0.19 \pm 0.28)(\mathrm{M/L})_\odot$. The estimated rest frame $(g-r) \simeq 0.85$ color of the host puts it in the "green valley"between the star forming "blue cloud" and the "red sequence" (see e.g. Strateva et al. 2001; Blanton et al. 2003), as seen in Figure 5.

The estimated MgII and C[IV] line FWHM are 49 and 21 Å, respectively (Fohlmeister et al. 2008, Morgan, private communication). These both indicate a black hole mass of $\log(M_{BH}/\mathrm{M}_\odot) \simeq 8.6$ based on the scalings of McClure & Jarvis (2002) for MgII and Vestergaard & Peterson (2006) for C[IV]. We have also applied the revised normalization of Onken et al. (2004) to the MgII estimate. The estimated magnification-corrected luminosity at rest-frame at 1350Å is 2.0×10^{45} erg/s based on power-law fits to the B, V, and I HST images. The uncertainties in the M_{BH} estimate are dominated by systematics, principally the 0.3 dex uncertainty typical of M_{BH} estimates from line widths and 0.15 dex from the magnification uncertainties. Nonetheless, the excellent agreement between the MgII and C[IV] mass estimates ($\log(M_{BH}/\mathrm{M}_\odot) = 8.62$ and 8.56, respectively) is reassuring. If we estimate a black hole mass from the rest frame V-band host luminosity of $(2.07 \pm 0.03) \times 10^{43}$ ergs/s, using the relation of Gültekin et al. (2009), we find a black hole mass of $\log(M_{BH}/M_\odot) = 8.74 \pm 0.21$ that agrees well with the estimates from the line widths. Note, however, that we have no estimate of the fraction of the luminosity due to the host's bulge. The Eddington luminosity for such a black hole is

$$L_{Edd} = 5.7 \times 10^{12} \left(\frac{M_{BH}}{10^{8.6} \mathrm{M}_\odot} \right) \mathrm{L}_\odot. \quad (3)$$

From our template models we can estimate the 0.1–24μm luminosity of the black hole (see Table 3). We use the 3μm to L_{IR} analysis from §2.6 of Gallagher et al. (2007), applied to the Boötes field AGNs to estimate a bolometric correction of BC$\simeq$1 between this luminosity and the bolometric luminosity (for an in depth discussion, see Assef et al. 2009).

Based on these scalings and a weighted average over the different lensed images, we estimate that the star formation rate is $\log(\dot{M}/\mathrm{M}_\odot\ \mathrm{yr}^{-1}) = 1.18 \pm 0.26$ compared to a stellar mass of $\log(M_\star/M_\odot) = 11.09 \pm 0.28$. The uncertainties in these quantities are dominated by the scatter in the scaling relations used to derive them. Aside from the systematic uncertainties in the scalings used to determine the SFR (40%, Kennicutt 1998; Bavouzet et al. 2008) and stellar mass (26%, Bell et al. 2003), the biggest uncertainties arise from the magnification estimates. The IRAC QSO mask flux ratios are probably a reasonable estimate of the intrinsic flux ratios and these are B/A$\sim$0.76, C/A$\sim$0.63, and D/A$\sim$0.32 compared to 0.67, 0.34, and 0.27 respectively from the Inada et al. (2008) models (Oguri, private communication). Much of this will be incorporated into the uncertainties estimated from

the scatter between the various lensed images and masks. The host SED has roughly equal contributions from the E and Sbc templates and little contribution from the Irr template, independent of the image or region fit. While dust could obscure the optical/UV emission of young stars in the Irr template (see Figure 4), we would not find a good fit to the host using an obscured Irr template. Note that the inner (QSO mask) and outer (Host mask) regions of the host galaxy seem to contain a similar number of stars and have similar specific star formation rates.

We can also compare these inferences about the stars to those for the black hole. The black hole represents a mass fraction of $\log(M_{BH}/M_\star) = -2.49 \pm 0.28$ compared to the stars, which is marginally inconsistent with local estimates of $\log(M_{BH}/M_\star) = -2.85 \pm 0.12$ (Häring & Rix 2004). Our result is in better agreement with the Peng et al. (2006a) estimate that the M_{BH}/M_* relation is 4^{+2}_{-1} ($\simeq 0.6$ dex) larger at $z = 1.7$ than locally (i.e. $\log(M_{BH}/M_\star) \simeq -2.25$). If so, the agreement of the black hole masses estimated from the line widths and the host luminosity is then a coincidence where the effect of evolution in the relation is balanced by over-estimating the bulge luminosity. Finally, we note that after including our estimate of the bolometric correction, we find that $L_{BH}/L_{Edd} \simeq 0.24 \pm 0.05$, so the black hole is radiating at a significant fraction of its Eddington limit, as is typical of quasars at this epoch (e.g. Kollmeier et al. 2006). The quasar may be moderately extincted, as we find best fits where the quasar template is reddened by $E(B-V) \simeq 0.1$, 0.1, 0.15, and 0.0 magnitudes for the A-D images, respectively.

In summary, both the host galaxy and quasar in SDSS J1004+4112 have relatively unremarkable properties. The one exception is that the host galaxy lies in the "green valley" and so may be in transition from being a star forming galaxy in the "blue cloud" to an old, red, and dead galaxy on the red sequence. This is consistent with the observation of Hickox et al. (2009) that many X-ray AGN with the X-ray luminosity of SDSS J1004+4112 ($\simeq 2\times10^{43}$ ergs/s, Ota et al. 2006; Lamer et al. 2006) lie in the green valley, while radio AGN tend to lie on the red sequence and mid-IR selected AGN tend to lie in the blue cloud. The extreme extension of the host galaxy should also make it possible to obtain spectroscopic observations of the host galaxy, potentially allowing measurement of the dynamical mass or metallicity.

We would like to thank Professor Chris Kochanek for his incredible patience and support in this venture. Special thanks also to Roberto Assef, Shawn Poindexter, and Dr. Emilio Falco for their assistance in this work. Thanks to C. Morgan and C. Peng for their comments and help on the estimated black hole mass. We would also like to thank D. Maoz and M. Oguri for their comments. This work is based in part on observations made with the NASA/ESA *Hubble Space Telescope*. Support for programs GO-9744, 10509 and 10716 was

provided by NASA through a grant from the Space Telescope Science Institute, which is operated by AURA, Inc., under NASA contract NAS5-2655. It is also based in part on observations made with the Spitzer Space Telescope, AO-20451, which is operated by the Jet Propulsion Laboratory, California Institute of Technology under a contract with NASA. Support for this program SST-20277 was provided by NASA through an award issued by JPL/Caltech. CSK is also supported by NSF grant AST-0708082.

REFERENCES

Adelman-McCarthy, J.K., et al. 2008, ApJS, 175, 297

Assef, R.J., et al. 2008, ApJ, 676, 286

Assef, R.J., et al. 2009, in preparation

Bavouzet, N., et al. 2008, arXiv:0712.0965v1 [astro-ph]

Bell, E.F., et al. 2003, ApJ, 149, 289

Blanton, M.R., et al. 2003, ApJ, 594, 186B

Di Matteo, T., et al. 2008, ApJ, 676, 33

Fohlmeister, J., et al., 2007, ApJ, 662, 62

Fohlmeister, J., et al. 2008, ApJ, 676, 761

Fruchter et al. 2002, PASP, 114, 144

Gallagher, S.C., et al. 2007, ApJ, 661, 30-37

Gültekin, K., et al. 2009, arXiv:0903.4897

Häring, N., Rix, H.-W. 2004, ApJ, 604, 89-92

Hickox, R.C., et al. 2009, arxiv: 0901.4121

Hopkins, P., et al. 2005a, ApJ, 625, 71

Hopkins, P., et al. 2005b, ApJ, 630, 705

Hopkins, P., Narayan, R., Hernquist, L. 2006, ApJ, 643, 641

Hopkins, P., et al. 2006, ApJS, 163, 1

Hopkins, P., et al. 2008, ApJS, 175, 356

Inada, N., et al. 2003, Nature, 426, 810-812

Inada, N., et al., 2005, PASJ, 57, 71

Inada, N., et al. 2008, PASJ, 60, 27

Jannuzi, B.T., Dey, A. 1999 AAS, 195, 1207J

Kauffmann, G., Heckman, T. 2005, RSPTA, 363, 621

Kennicutt Jr., R.C. 1998, ApJ, 498, 541

Kochanek, C.S., et al. 2008, in preparation

Kollmeier, J., et al. 2006, ApJ, 648, 128

Lamer et al. 2006, A&A, 454, 493

Lauer, T., et al. 2007, ApJ, 670, 249

Lehár, J., et al. 2000, ApJ, 536, 584

Marconi, A., Hunt, L. 2003, ApJ, 589, 21

McClure & Jarvis, 2002, MNRAS, 337, 109

Oguri, M., Private communication with C.S. Kochanek 2008/07/22

Onken, C., et al. 2004, ApJ, 615, 645

Ota, N., et al., 2006, ApJ, 647, 215

Peng, C.Y., et al. 2006a, ApJ, 640, 114

Peng, C.Y., et al. 2006b, ApJ, 649, 616

Peng, C.Y., et al. 2006c, New Astron.Rev. 50, 689-693

Sharon, K., et al. 2005, ApJ, 629, 73

Sijacki, D., et al. 2007, MNRAS, 380, 877-900

Strateva, I., et al. 2001, AJ, 122, 1861S

Vanden Berk et al. 2004, ApJ, 601, 692

Vestergaard & Peterson, 2006, ApJ, 641, 689

Table 1. Observations of SDSS J1004+4112

Program	Instrument	Filter	Date	Exposure Time (sec)
HST-9744	NICMOS/NIC2	H(F160W)	2004/04/28	2688*
	NICMOS/NIC2	H(F160W)	2004/10/09	2688
HST-10716	NICMOS/NIC2	H(F160W)	2006/10/22	2688
HST-10509	ACS/WFC	B(F435W)	2005/12/13	13378
HST-9744	ACS/WFC	V(F555W)	2004/01/28	2025
HST-10509	ACS/WFC	V(F555W)	2005/12/12	7978
HST-9744	ACS/WFC	I(F814W)	2004/04/28	2025
HST-10509	ACS/WFC	I(F814W)	2005/12/12	5360
SST-20277	IRAC	3.6–8.0μm	2005/12/08, 2005/12/26, 2006/11/25	7494

Note. — *This observation includes only images A and B.

Table 2. SDSS J1004+4112 Magnitudes

Filter	Date	Image A host	Image A qso	Image A joint	Image B host	Image B qso	Image B joint	Image C host	Image C qso	Image C joint	Image D joint
B	2005/12/13	28.18±0.81	23.44±0.03	23.42±0.01	28.55±0.67	23.24±0.03	23.22±0.01	26.43±0.86	22.67±0.57	22.64±0.45	22.87±0.36
V	2004/01/28	27.93±1.12	23.36±0.15	23.34±0.13	27.39±1.18	23.29±0.15	23.26±0.13	26.34±1.25	22.65±0.15	22.61±0.15	22.41±0.14
V	2005/12/12	27.76±1.11	23.29±0.10	23.27±0.08	27.59±1.19	23.27±0.11	23.24±0.08	26.69±1.09	22.62±0.11	22.59±0.08	22.73±0.08
I	2004/04/28	25.52±0.97	22.30±0.16	22.26±0.16	25.39±0.81	22.16±0.16	22.11±0.15	24.73±0.65	21.48±0.16	21.41±0.16	21.86±0.16
I	2005/12/12	25.78±0.73	22.42±0.10	22.36±0.04	25.57±0.72	22.27±0.12	22.21±0.04	24.65±0.61	21.83±0.24	21.76±0.19	21.64±0.03
H	2004/04/28	22.43±0.23	21.26±0.10	21.02±0.11	22.36±0.14	21.09±0.11	20.86±0.11	...	...	...	...
H	2004/10/09	22.41±0.41	20.93±0.08	20.66±0.13	21.89±0.40	20.88±0.09	20.47±0.14	21.36±0.40	20.05±0.10	19.64±0.15	19.85±0.13
H	2006/10/22	22.38±0.15	21.16±0.10	20.87±0.09	21.94±0.33	20.86±0.10	20.48±0.13	21.79±0.37	20.53±0.08	20.21±0.11	20.20±0.10
3.6μm	2005/12/08	19.94±0.33	18.69±0.01	18.30±0.05	19.42±0.21	18.60±0.03	18.07±0.09	19.05±0.58	18.11±0.04	17.64±0.16	17.79±0.17
3.6μm	2005/12/26	19.80±0.17	18.72±0.02	18.29±0.07	19.41±0.33	18.65±0.02	18.10±0.10	19.18±0.34	18.05±0.02	17.62±0.06	17.77±0.04
3.6μm	2006/11/25	19.80±0.22	18.86±0.06	18.42±0.10	19.37±0.32	18.67±0.06	18.10±0.07	18.96±0.22	18.07±0.06	17.58±0.08	17.71±0.06
4.5μm	2005/12/08	19.12±0.23	17.87±0.01	17.46±0.06	18.90±0.11	17.74±0.02	17.32±0.03	18.14±0.07	17.36±0.02	16.83±0.03	17.07±0.04
4.5μm	2005/12/26	19.01±0.22	17.92±0.02	17.47±0.03	18.86±0.08	17.81±0.02	17.36±0.03	18.16±0.15	17.34±0.02	16.81±0.07	17.08±0.02
4.5μm	2006/11/25	19.04±0.22	18.01±0.05	17.59±0.05	18.89±0.04	17.85±0.05	17.43±0.05	18.07±0.21	17.41±0.05	16.87±0.06	16.99±0.05
5.8μm	2005/12/08	18.92±0.32	17.03±0.01	16.71±0.03	18.60±0.15	16.96±0.02	16.62±0.06	18.09±0.23	16.49±0.01	16.15±0.02	16.40±0.03
5.8μm	2005/12/26	19.08±0.40	17.06±0.01	16.76±0.04	18.87±0.18	16.96±0.01	16.65±0.03	18.15±0.13	16.46±0.01	16.12±0.02	16.41±0.02
5.8μm	2006/11/25	18.95±0.40	17.12±0.04	16.90±0.06	18.77±0.22	16.91±0.04	16.70±0.05	18.04±0.15	16.42±0.04	16.22±0.07	16.35±0.04
8.0μm	2005/12/08	18.53±0.17	15.93±0.01	15.89±0.01	18.27±0.48	15.85±0.01	15.80±0.02	17.96±0.32	15.31±0.01	15.38±0.01	15.73±0.02
8.0μm	2005/12/26	18.51±0.18	16.07±0.01	15.88±0.02	18.45±0.30	16.00±0.01	15.85±0.03	17.87±0.14	15.49±0.01	15.38±0.01	15.71±0.02
8.0μm	2006/11/25	18.46±0.08	15.87±0.03	16.02±0.03	18.27±0.23	15.73±0.03	15.91±0.04	17.78±0.09	15.11±0.03	15.45±0.03	15.66±0.04

Note. — These are Vega magnitudes corrected for magnification by the lens based on the models of Inada et al. (2008, Oguri private communication). The fluxes in the QSO mask contain a portion of the host galaxy. The QSO and joint fluxes are adjusted to account for time-dependent variability in the quasar using corrections from the monitoring data of Fohlmeister et al. (2008). The 2004/04/28 NICMOS H-band observation included only images A and B.

Table 3. Magnification Corrected Properties

Image	Mask	E	Sbc	Irr	QSO	SFR	$(M/L)_K$	$M_\star$
		(Luminosity in units of $10^{10}L_\odot$)				($M_\odot\,yr^{-1}$)	Solar Units	($10^{10}M_\odot$)
A	host	1.05±0.64	2.84±0.95	0.038±0.120	≡0	8.8±4.0	0.605±0.100	4.3±0.7
	qso	1.35±0.01	1.93±0.01	0.104±0.001	145.6±0.2	6.5±2.4	0.597±0.105	1.9±0.4
	joint	2.87±0.06	4.09±0.09	0.219±0.005	125.7±0.7	12.1±4.5	0.578±0.100	8.4±1.0
B	host	2.02±1.04	1.86±1.72	0.049±0.133	≡0	6.3±5.1	0.612±0.100	4.9±0.6
	qso	1.40±0.01	1.99±0.01	0.107±0.001	167.0±0.2	6.7±2.5	0.591±0.101	5.6±0.8
	joint	4.69±0.06	6.67±0.09	0.358±0.005	108.9±0.8	18.2±6.8	0.575±0.100	13.6±1.5
C	host	4.06±1.49	2.57±2.25	0.685±0.448	≡0	8.9±6.4	0.610±0.100	9.0±1.4
	qso	3.00±0.02	4.26±0.02	0.229±0.010	250.7±0.6	12.6±4.7	0.595±0.103	7.3±0.8
	joint	8.57±0.17	12.19±0.24	0.655±0.013	166.6±1.7	30.1±11.1	0.590±0.101	24.9±2.8
D	joint	7.42±0.07	10.55±0.10	0.567±0.005	126.2±1.4	26.7±9.9	0.621±0.102	21.6±2.2
Avg	host	1.64±0.51	2.60±0.78	0.067±0.087	≡0	8.1±2.8	0.609±0.058	5.1±0.5
	qso	1.81±0.03	1.96±0.03	0.165±0.003	155.0±0.6	4.8±1.0	0.594±0.059	3.4±0.3
	joint	5.54±0.04	6.01±0.04	0.505±0.003	124.0±0.5	15.0±3.0	0.591±0.050	12.3±0.7

Note. — Contribution of each template to the SED. These are corrected for magnification based on the models of Inada et al. (2008, Oguri private communication). The star formation rate (SFR) and stellar mass are estimated as described in §3. Note that the average values at the bottom of the table (Avg) are uncertainty weighted averages of the corresponding values for the individual components.

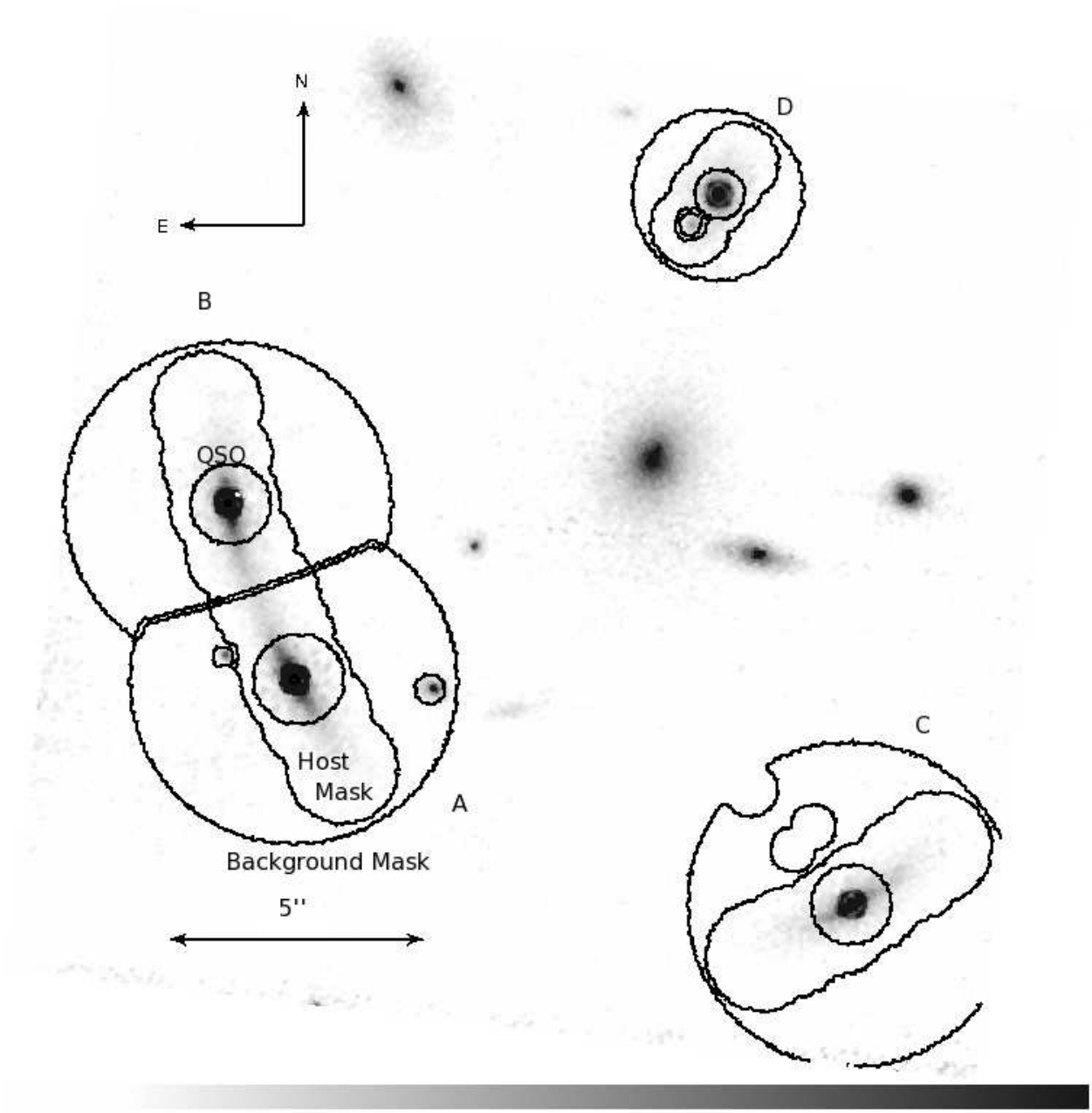

Fig. 1.— NICMOS/NIC2 H-band (F160W) image of SDSS J1004+4112 with mask outlines denoted by the solid black lines. The host galaxy is clearly seen stretched out from beneath the peak of the QSO. For image D we only use the joint mask.

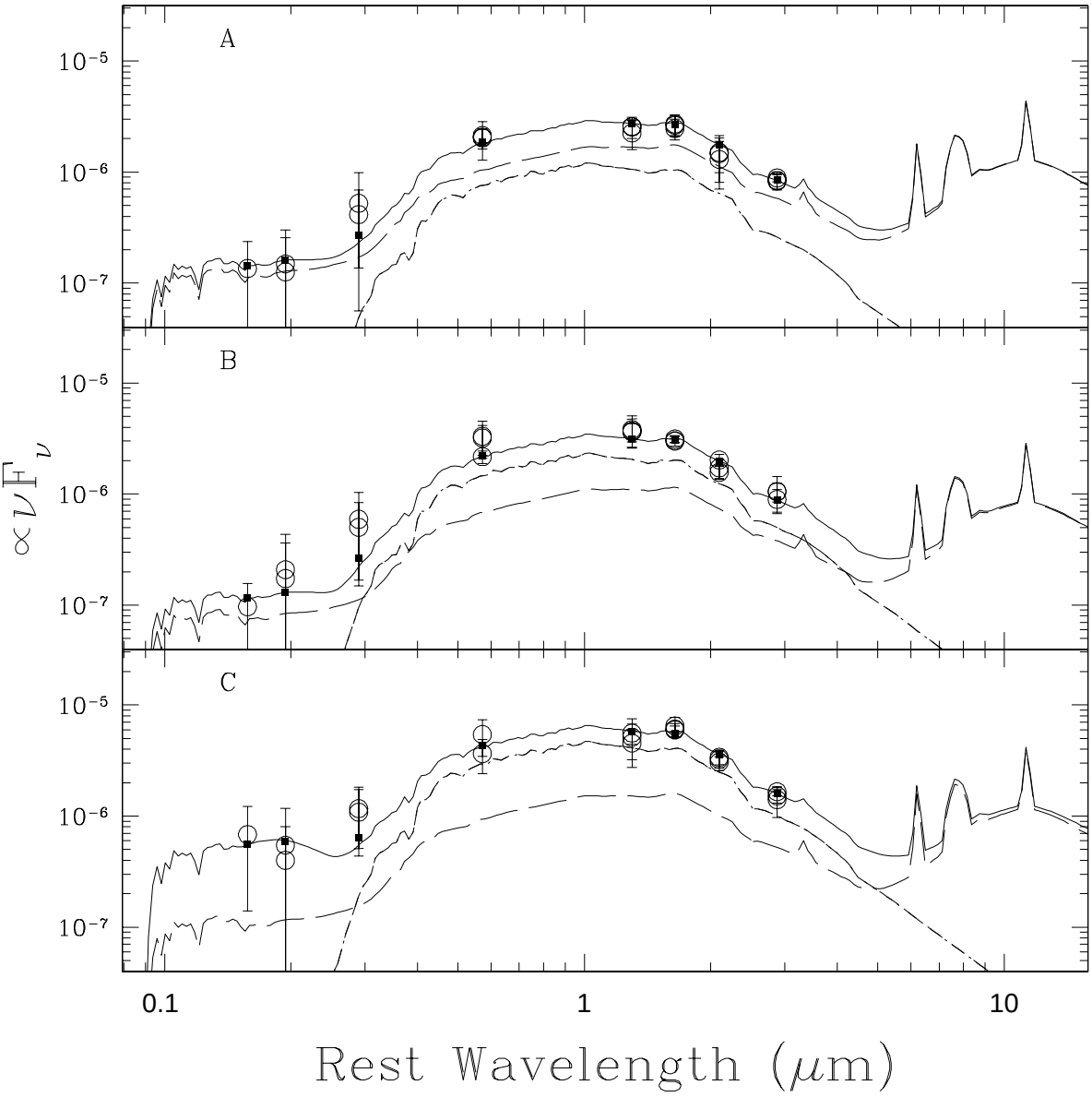

Fig. 2.— Host mask spectral energy distribution for images A (Top), B (Middle), and C (Bottom). Observation bands are, from left to right, ACS/WFC B(F435W), V(F555W), I(F814W), NICMOS/NIC2 H(F160W), IRAC 3.6, 4.5, 5.8, and 8.0 μm. The results for all observation epochs are shown. The solid, dot-dashed, long-dashed, and short-dashed lines correspond to the total SED and the contribution from the E, Sbc, and Irr templates respectively. The open circles are the measured fluxes while the closed squares are the best fit value given the template fits. The contribution from the Irr template is too small to be seen on this scale. The SEDs are corrected for magnification by the lens based on the models of Inada et al. (2008, Oguri private communication).

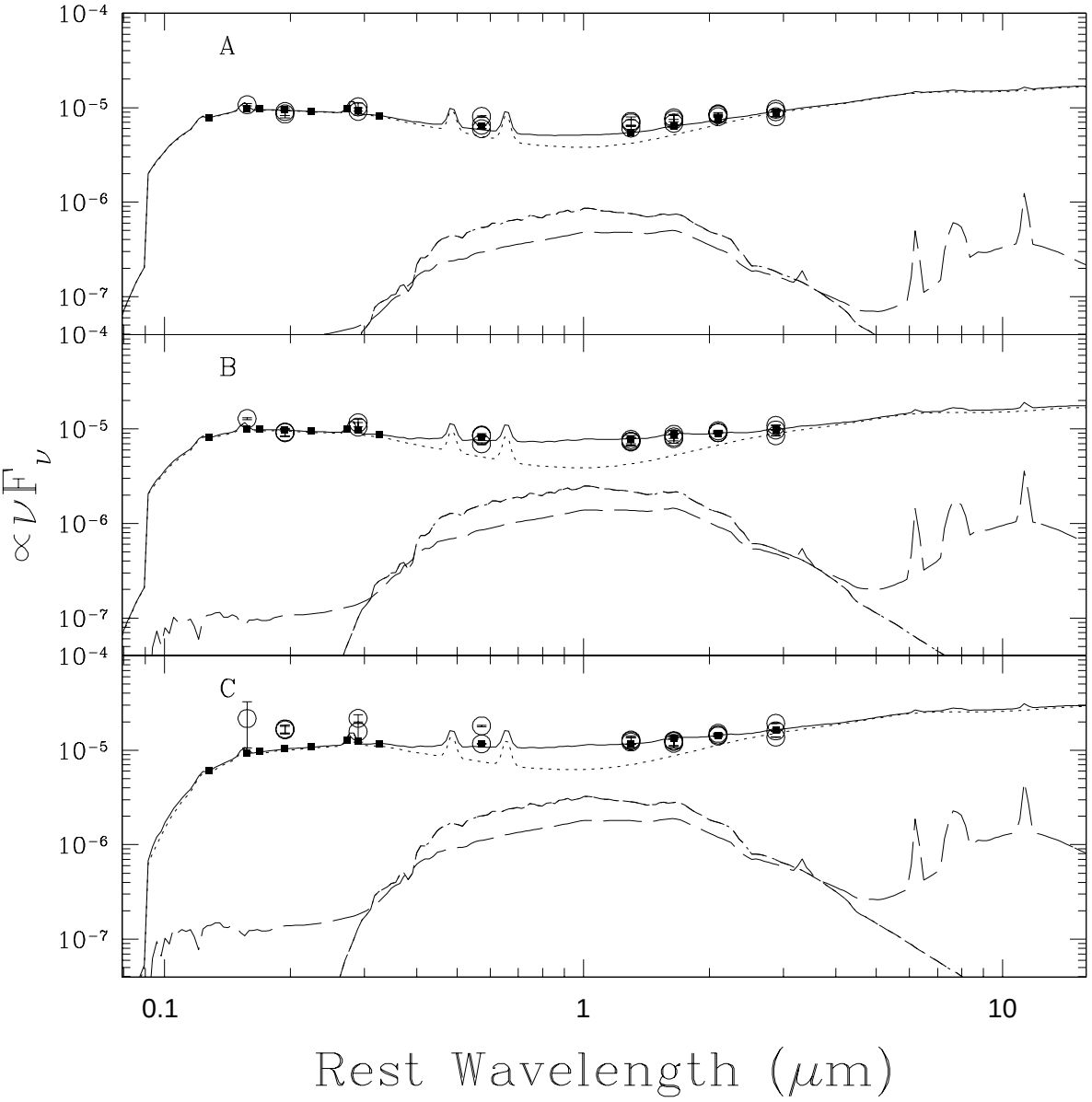

Fig. 3.— QSO mask spectral energy distribution for images A (Top), B (Middle), and C (Bottom). The galaxy templates and data points are represented as described in Figure 2 while the dotted line shows the QSO template and the solid line shows the sum of all templates. The contribution from the Irr template is too small to be seen on this scale. The changes in the optical continuum slope are due to the variations in the QSO extinction estimates.

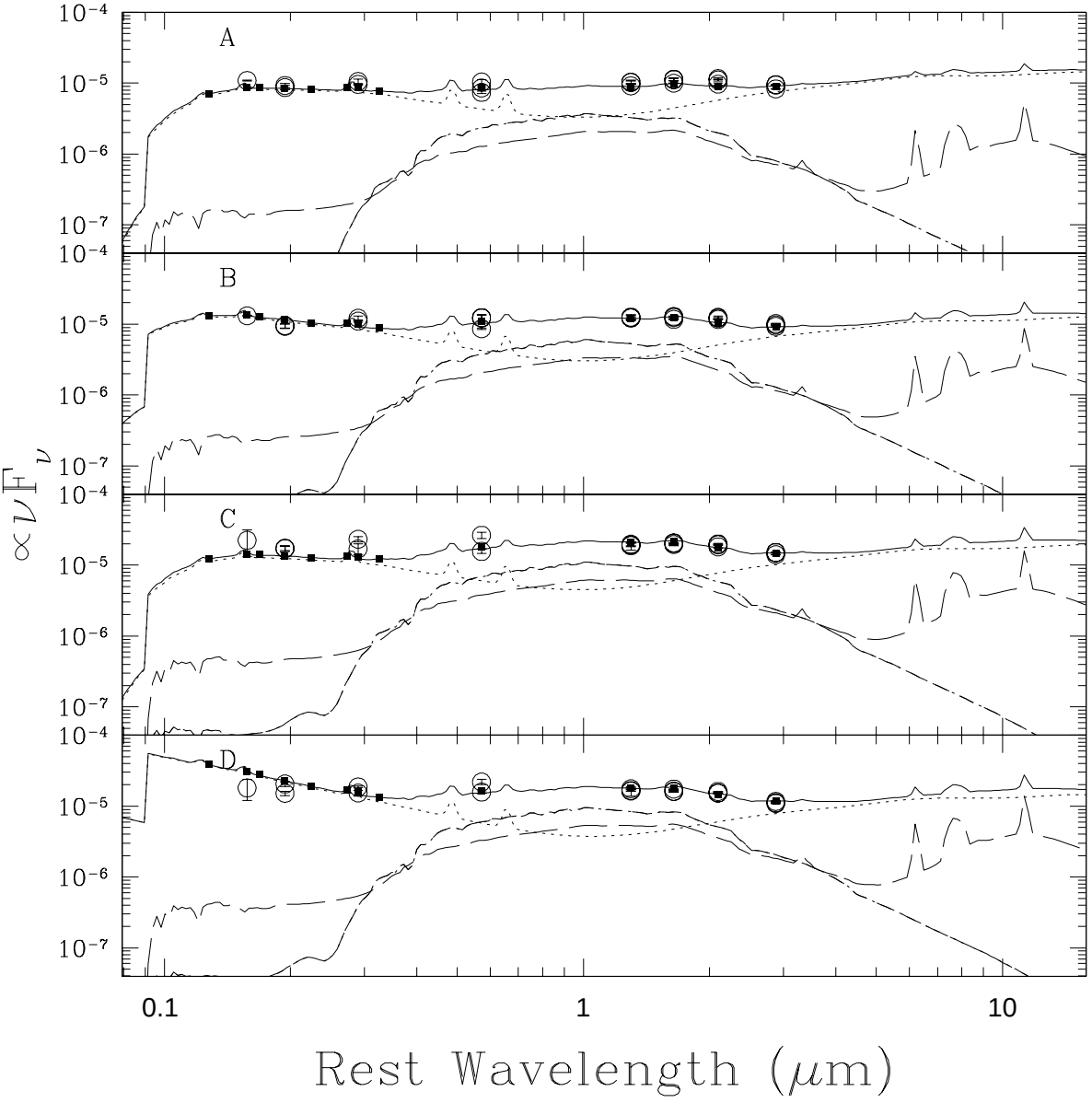

Fig. 4.— Joint mask (QSO + Host) spectral energy distribution for images A (Top), B (Top Middle), C (Bottom Middle), and D (Bottom). The components are as described in Figs. 2 and 3. The contribution from the Irr template is too small to be seen on this scale. Note that the template models show some variation in the amount of extinction accounted for in the various images.

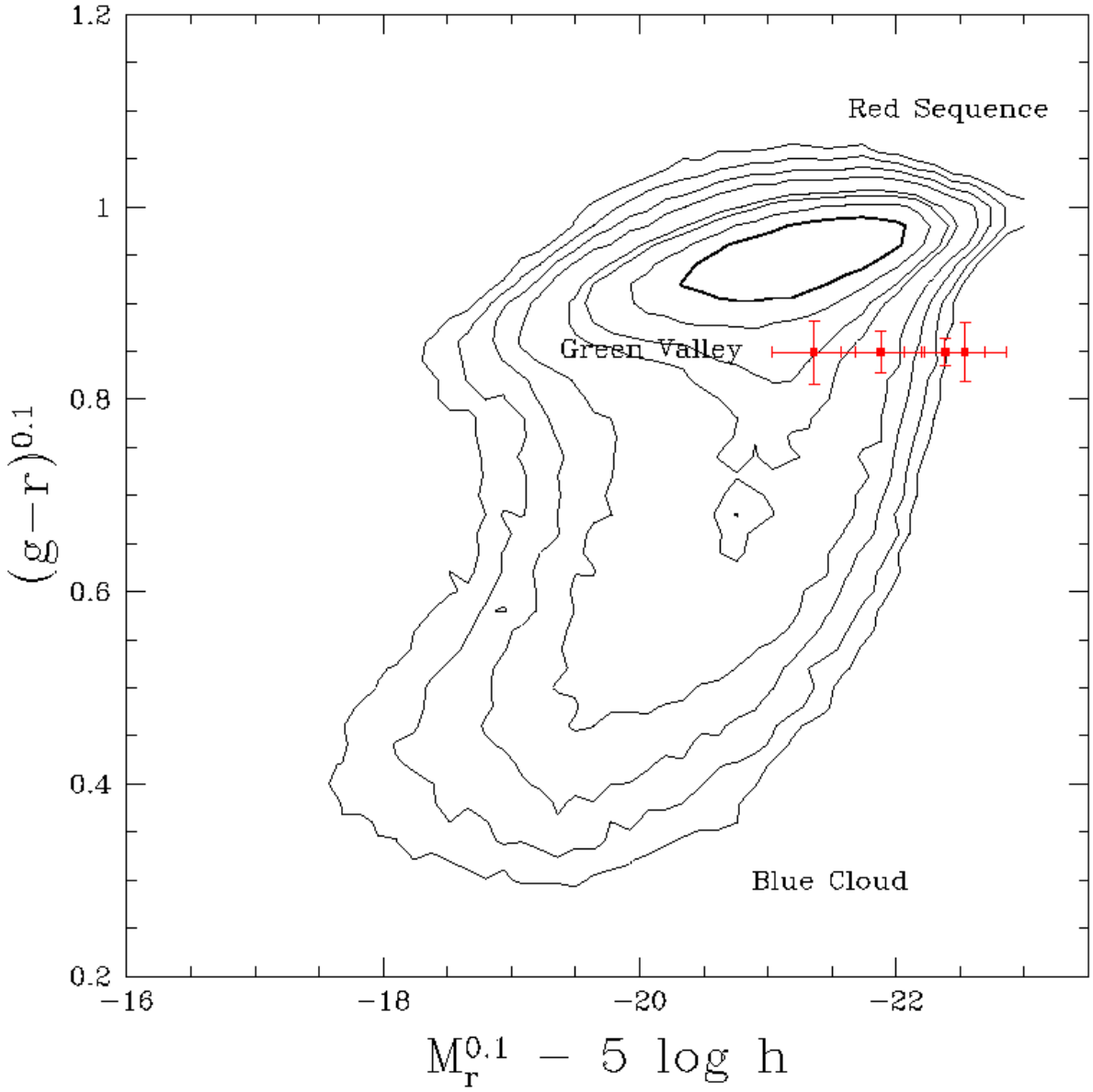

Fig. 5.— Color-magnitude diagram of SDSS galaxies from the SDSS Data Release 6 (Adelman-McCarthy et al. 2008) with the points for the four images of SDSS J1004+4112 in red. The systematic effects on the luminosity from estimates of the magnification for each lensed image is clearly seen from the similarity in color as compared to the factor of $\simeq 2$ differences in the estimates of the magnification-corrected luminosity.